HHS Public Access

Author manuscript

Oncogene. Author manuscript; available in PMC 2019 September 27.

Published in final edited form as:

Oncogene. 2019 June ; 38(26): 5308–5320. doi:10.1038/s41388-019-0794-6.

Inhibition of geranylgeranyl diphosphate synthase is a novel therapeutic strategy for pancreatic ductal adenocarcinoma

Staci L. Haney[1,2], **Michelle L. Varney**[1,2], **Yashpal S. Chhonker**[3], **Simon Shin**[2,4], **Kamiya Mehla**[2,4], **Ayrianne J. Crawford**[2,4], **Heather Jensen Smith**[2,4], **Lynette M. Smith**[5], **Daryl J. Murry**[2,3], **Michael A. Hollingsworth**[2,4], and **Sarah A. Holstein**[1,2,*]

[1]Department of Internal Medicine, University of Nebraska Medical Center, Omaha, NE, USA

[2]Fred & Pamela Buffett Cancer Center, University of Nebraska Medical Center, Omaha, NE, USA

[3]Department of Pharmacy Practice, University of Nebraska Medical Center, Omaha, NE, USA

[4]Eppley Institute for Research in Cancer, University of Nebraska Medical Center, Omaha, NE, USA

[5]College of Public Health, University of Nebraska Medical Center, Omaha, NE, USA

Abstract

Rab proteins play an essential role in regulating intracellular membrane trafficking processes. Rab activity is dependent upon geranylgeranylation, a post-translational modification that involves the addition of 20-carbon isoprenoid chains via the enzyme geranylgeranyl transferase (GGTase) II. We have focused on the development of inhibitors against geranylgeranyl diphosphate synthase (GGDPS), which generates the isoprenoid donor (GGPP), as anti-Rab agents. Pancreatic ductal adenocarcinoma (PDAC) is characterized by abnormal mucin production and these mucins play important roles in tumor development, metastasis and chemo-resistance. We hypothesized that GGDPS inhibitor (GGDPSi) treatment would induce PDAC cell death by disrupting mucin trafficking, thereby inducing the unfolded protein response pathway (UPR) and apoptosis. To this end, we evaluated the effects of RAM2061, a potent GGDPSi, against PDAC. Our studies revealed that GGDPSi treatment activates the UPR and triggers apoptosis in a variety of human and mouse PDAC cell lines. Furthermore, GGDPSi treatment was found to disrupt the intracellular trafficking of key mucins such as MUC1. These effects could be recapitulated by incubation with a specific GGTase II inhibitor, but not a GGTase I inhibitor, consistent with the effect being dependent on disruption of Rab-mediated activities. In addition, siRNA-mediated knockdown of GGDPS induces upregulation of UPR markers and disrupts MUC1 trafficking in PDAC cells. Experiments in two mouse models of PDAC demonstrated that GGDPSi treatment significantly slows tumor growth. Collectively, these data support further development of GGDPSi therapy as a novel strategy for the treatment of PDAC.

*Corresponding Author: Sarah A. Holstein, MD, PhD, Department of Internal Medicine, University of Nebraska Medical Center, 986840 Nebraska Medical Center, Omaha, NE 68198, Tel: 402-559-8500, Fax: 402-559-6520, sarah.holstein@unmc.edu.

Conflict of Interest. The authors have no relevant conflicts of interest to disclose

Keywords

pancreatic ductal adenocarcinoma; Rab; geranylgeranyl diphosphate synthase inhibitor; unfolded protein response pathway; apoptosis; mucin

Introduction

Pancreatic ductal adenocarcinoma (PDAC) is an aggressive malignancy with a 5-year survival of only 7% [1]. Late diagnosis, high metastatic rates and chemotherapy resistance are all responsible for the dismal outcomes. Surgery is potentially curable for early stage disease, but the vast majority of patients present with advanced disease and are thus ineligible. Therefore, novel treatment strategies are desperately needed. PDAC is characterized by aberrant expression, glycosylation and localization of mucins [2]. Mucins play a causal role in various aspects of PDAC pathology, including metastasis, immune evasion, drug resistance and tumor growth [3–5]. Upregulation of several mucins in PDAC patients predict poor prognosis, including MUC1, MUC4, MUC16, MUC2, MUC5AC/AB, and MUC13 [2]. The mucin family is complex, consisting of 21 members that are categorized as secreted and transmembrane mucins. Clinical trials have largely focused on targeting single mucins, such a MUC1, through immunotherapy with minimal success [6]. However, agents that target mucin activity as a whole, such as by blocking their trafficking, have not previously been explored.

Rab proteins are key regulators of nearly all aspects of intracellular protein trafficking, including vesicle budding, movement, docking and fusion. In order to be active, Rab proteins must undergo a post-translational modification termed geranylgeranylation. In the isoprenoid biosynthesis pathway (IBP), the enzyme geranylgeranyl diphosphate synthase (GGDPS) generates the 20-carbon isoprenoid termed geranylgeranyl pyrophosphate (GGPP). The enzyme geranylgeranyl transferase II (GGTase II) then covalently links GGPP to Rabs. We have focused on the development of GGDPS inhibitors as anti-Rab agents [7]. Our previous work has identified several isoprenoid triazole bisphosphonates, including VSW1198 (a mixture of homogeranyl and homoneryl isomers) [8, 9] and RAM2061 (an α-methyl substituted homoneryl triazole bisphosphonate) [10] that are potent and selective GGDPS inhibitors (GGDPSi) (Fig. 1A). We have previously demonstrated that the strategy of targeting intracellular trafficking processes with GGDPSi blocks monoclonal protein secretion and promotes apoptosis in multiple myeloma cells [11, 12]. Whether GGDPSi treatment may be relevant to other malignancies characterized by aberrant protein production/secretion has yet to be determined.

In the present study, we hypothesized that GGDPSi treatment would impair protein trafficking, causing ER stress and activating the unfolded protein response pathway (UPR) and apoptosis in PDAC. To this end, we have evaluated the activity of RAM2061 in human and mouse PDAC cell lines. Consistent with our hypothesis, we have found that GGDPS inhibition impairs mucin trafficking and induces the UPR to trigger apoptotic cell death in PDAC cells. Furthermore, using mouse models of pancreatic cancer we demonstrate that GGDPSi treatment slows tumor growth *in vivo*. Collectively, these studies illustrate that

disruption of Rab activity via GGDPSi represents an innovative mechanism by which to target PDAC.

Results

RAM2061 inhibits geranylgeranylation in human and mouse PDAC cell lines.

Rap1a is a representative geranylgeranylated protein that can be readily identified by immunoblot using an antibody that recognizes only the non-prenylated protein [9]. Incubation with RAM2061 resulted in accumulation of unmodified Rap1a in a concentration-dependent manner across a panel of human (Fig. 1B) and mouse (Fig. 1C) cell lines. Consistent with the mechanisms of action of this inhibitor, RAM2061 treatment reduces intracellular GGPP levels and increases intracellular FPP levels (Fig. 1D). qRT-PCR analysis showed no change in the expression levels of GGDPS upon RAM2061 treatment (Supplemental Fig. 1).

Inhibition of GGDPS induces apoptosis of PDAC cells.

Immunoblot analysis revealed that four out of six human PDAC cell lines treated with RAM2061 show increased PARP cleavage and that all six cell lines had accumulation of at least one cleaved caspase at 48 or 72 hours (Fig. 2A). A similar activation of caspase cleavage was observed in mouse KPC cell lines following incubation with RAM2061 (Fig. 2B). MTT assays demonstrated concentration-dependent cytotoxic effects of RAM2061 in human and mouse PDAC cell lines (Fig. 3A, B). Flow cytometry studies using AnnexinV and propidium iodide confirm that GGDPSi treatment increases the early and late stage apoptotic cellular populations in a concentration-dependent manner (Fig. 3C). Collectively, these data demonstrate that GGDPSi treatment induces apoptotic cell death in PDAC cell lines.

Disruption of protein geranylgeranylation activates the UPR pathway.

To determine if GGDPSi treatment promotes ER stress and induction of the UPR, we evaluated markers of the UPR via immunoblot analysis. We found that RAM2061 induces accumulation of ATF4, IRE1α, and phosphorylated eIF2α in a concentration-dependent manner in both human and mouse PDAC cells at either 48 or 72 hours (Fig. 4A, B). We also found that RAM2061 induced cleavage of XBP-1 mRNA from its inactive to its active form (Fig. 4C). Likewise, qRT-PCR analysis showed upregulation in the expression of ATF4, ATF6, CHOP and PERK following GGDPSi treatment (Fig. 4D). Furthermore, siRNA mediated knockdown of GGDPS induces upregulation of UPR markers relative to control scrambled siRNA in three PDAC cell lines (Supplemental Fig. 2).

Reduction in cellular GGPP and disruption of Rab geranylgeranylation mediate RAM2061-induced UPR and apoptosis activation.

To determine if a decrease in cellular GGPP levels are responsible for the observed effects on the UPR and apoptosis, we performed add-back experiments with GGPP in the presence or absence of RAM2061. Immunoblot analysis confirmed that co-incubation of RAM2061 with GGPP completely abrogates the upregulation of UPR and apoptotic markers (Fig. 5A). As GGDPS inhibition results in the global disruption of protein geranylgeranylation, we

performed studies utilizing specific inhibitors of GGTase I and GGTase II in order to determine whether the effects of RAM2061 are due to disruption of Rab-mediated processes (i.e., GGTase II) or non-Rab-mediated processes (i.e., GGTase I). Only in the cells treated with GGDPS or GGTase II inhibitors, but not GGTase I inhibitor, did we observe an increase in UPR and apoptosis markers (Fig. 5B). Similar to GGDPSi treatment, GGTase II inhibition also results in cytotoxic effects as determined by an MTT assay (Supplemental Fig. 3). Collectively, these data suggest that the effects of RAM2061 are due to depletion of GGPP and disruption of Rab geranylgeranylation and that this mechanism is responsible for the observed cytotoxic effects.

Inhibition of Rab geranylgeranylation disrupts mucin trafficking.

PDAC cells are characterized by the production of abnormal mucins which play many pathological roles. We were therefore interested in determining whether inhibition of Rab geranylgeranylation would disrupt mucin trafficking. Using immunoblot analysis we assessed levels of MUC1, MUC5ac and MUC16 in human PDAC cells following GGDPSi treatment. For MUC1, two antibodies were utilized: one that recognizes the TnSTn tumor epitope and one that recognizes an aberrant underglycosylated form [13, 14]. Incubation with RAM2061 caused retention of mucins within the cell in a concentration-dependent manner at both 48 and 72 hours (Fig. 6A, and Supplemental Fig. 4,5). The pattern observed, particularly for the MUC1 blots, is consistent with the accumulation of variably glycosylated forms [15]. Incubation with a GGTase II inhibitor, but not a GGTase I inhibitor, produced a similar retention of MUC1 protein inside the cell (Fig. 6B), demonstrating the dependence of this effect on disruption of Rab activity. In RAM2061-treated cells, confocal microscopy revealed that in contrast to untreated cells, the majority of MUC1 was co-localized with the Golgi (Fig. 6C). Immunoblot analysis of cells treated with brefeldin A (BFA), a known inhibitor of ER to Golgi transport [16], revealed no increase in intracellular MUC1 (Supplemental Fig. 6). In aggregate, these studies suggest that the observed accumulation of MUC1 (as assessed by these particular epitopes) induced by RAM2061 is occurring beyond the ER, however the possibility that less processed forms of MUC1 are being retained in the ER is not excluded. Using flow cytometry, we observed a decrease in the cell surface levels of MUC1 in MIA PaCa-2 and BxPC-3 cell lines following incubation with RAM2061 (Fig. 6D). No change in the mRNA levels of MUC1 were observed following GGDPSi treatment (Supplemental Fig. 7). Furthermore, siRNA mediated knockdown of GGDPS induced disruption of MUC1 trafficking within BxPC-3 and Capan-1 cells (Supplemental Fig. 8). Finally, incubation with RAM2061 reduced cellular invasion through matrigel-coated transwells in AsPC-1 and MIA PaCa-2 cells (Fig. 7).

GGDPSi treatment slows PDAC tumor growth *in vivo*.

Using two mouse models of pancreatic cancer, we evaluated whether twice-weekly treatment with VSW1198 (an analogue of RAM2061 that we have previously characterized in preclinical studies [9]) would be efficacious in slowing tumor growth *in vivo*. In a xenograft model where BxPC-3 cells were injected in the flanks of NOD-SCID mice, GGDPSi treatment significantly slowed tumor growth as compared to the vehicle-only control (Fig. 8A). Furthermore, in a KPC orthotopic model where PDAC cells are grown in the pancreata of syngeneic C57Bl/6 mice, VSW1198 treatment resulted in a smaller tumor

burden at the time of sacrifice as compared to the control mice (Fig. 8B). Ki67 staining of tumor sections demonstrate reduced cellular proliferation in tumors isolated from mice injected with VSW1198 relative to control animals (Fig 8C). In addition, accumulation of unmodified Rap1a was observed in the liver and tumors of mice within the treatment group, demonstrating disruption of geranylgeranylation was achieved (Fig. 8D). Collectively, these data illustrate efficacy of GGDPSi therapy *in vivo*.

Discussion

Our work represents the first studies to evaluate the activity of GGDPSi therapy against PDAC. We demonstrate that GGDPSi treatment induces markers of the UPR, triggers apoptotic cell death, disrupts mucin trafficking and impairs cellular invasion. Furthermore, we demonstrate positive efficacy data for GGDPSi treatment in two mouse models of PDAC.

Notably the human cell lines utilized in our studies represent varying degrees of differentiation (AsPC-1/MIA Paca2/PANC-1 = poorly differentiated; BxPC-3 =moderate to poorly differentiated; Capan-1 = well-differentiated) as well as different K-Ras, TP53, CDKN2A/p16 and SMAD4/DPC4 mutational profiles [17]. Rab inhibition, via either GGDPS or GGTase II inhibition, resulted in cytotoxic effects across all tested cell lines, including the mouse KPC cells, consistent with the efficacy of this therapeutic strategy being independent of the presence or absence of the more common driving mutations. GGDPS, as part of the IBP, is ubiquitously expressed in mammalian cells. There has been only one report evaluating GGDPS expression in malignancies. In this study, it was demonstrated that GGDPS expression in hepatocellular carcinoma specimens is higher (mRNA and protein) compared to surrounding healthy tissue [18]. Whether GGDPS expression differs significantly between PDAC cells and normal pancreatic cells is not known. However, our work demonstrates that our GGDPSi potently diminishes intracellular GGPP levels across all tested human PDAC cell lines and that it does not induce an upregulation of GGDPS expression, which could have been a potential mechanism for resistance. Finally, there is also evidence that Rab5 overexpression is associated with pancreatic cancer progression and poorer prognosis [19, 20], thus this may be another mechanism by which Rab inhibition in PDAC could be advantageous.

While both GGDPS and Rabs are found in all cell types, our work has shown that malignancies characterized by dependence on intact intracellular trafficking processes and protein secretion are inherently more sensitive to anti-Rab agents [11]. Our preclinical studies with the GGDPSi VSW1198, demonstrated the safety and feasibility of systemic GGDPSi therapy [9]. In particular, no evidence of hematologic, renal, cardiac, or neurologic toxicity was observed after repeat dosing of VSW1198 [9]. The dose limiting toxicity was hepatic in nature, likely a consequence of higher drug levels in the liver [9]. This hepatic uptake would be expected to be advantageous with respect to advanced PDAC which almost uniformly metastasizes to the liver.

MUC1 is largely regarded as an oncogene in pancreatic malignancies, where it has been shown to play a causal role proliferation, invasion, chemo-resistance, and angiogenesis [21]. Tumor associated MUC1 differs both in its subcellular localization as well as its

glycosylation state. Using antibodies that detect tumor specific MUC1 glycosylation states (TnSTn and underglycosylated), we found that MUC1 was accumulated within the cell upon GGDPSi treatment, suggesting disruption in its normal trafficking. Microscopy confirmed that MUC1 was co-localized within the Golgi upon GGDPSi treatment. We also observed disruption in MUC5ac and MUC16 trafficking following inhibition of GGDPS. There is evidence of a complex interaction between Rabs and mucins. For example, Rab5 was shown to regulate MUC1 internalization into clathrin-coated vesicles [22]. Jin et al described that MUC1 and Rab31 participate in a feedback loop that promotes the upregulation of MUC1 in breast cancer cells [23]. Others have reported that inhibition of MUC1 palmitoylation causes its accumulation in Rab11-positive endosomes and disrupted recycling [24]. Therefore, there is rationale for the development of small molecular inhibitors that target Rab-mediated trafficking events which could be used to disrupt the oncogenic activity of mucins in PDAC cells.

A number of studies have investigated the potential of mucin-based peptide vaccines, adoptive immunotherapy strategies or anti-mucin antibodies, but thus far have not been successful (reviewed in [25]). The sensitivity of pancreatic cancer cells *in vitro* to the proteasome inhibitor bortezomib was shown to be related to the degree of mucin production [26]. While bortezomib does induce the UPR, it would not be predicted to have an effect on mucin trafficking or secretion, thus it is perhaps not surprising that this agent has not been shown to be efficacious for this malignancy *in vivo* [27, 28]. In contrast, with GGDPS inhibition and resulting disruption of Rab activity, the potential benefits of blocking intracellular trafficking are two-fold: to induce the UPR and to disrupt mucin trafficking and function. The latter would be predicted to have beneficial effects with respect to inhibiting tumor development, progression and chemotherapy sensitivity while the former would result in selective toxicity to malignant pancreatic cells.

In summary, we have shown that the strategy of targeting Rab geranylgeranylation by inhibiting GGDPS induces the UPR and apoptosis *in vitro* and slows pancreatic tumor growth *in vivo*. Future studies will focus further on the functional consequences of disrupting mucin trafficking via GGDPS inhibition, including effects on chemo-resistance, tumor development and metastasis. Whether GGDPS inhibition exerts effects in PDAC cells that are independent of the UPR and mucin trafficking remains to be determined. Finally, it will also be important to explore the effects of combining GGDPSi therapy with other drugs relevant to the treatment of PDAC, including traditional cytotoxic chemotherapeutic agents as well as epidermal growth factor receptor-targeted therapy.

Materials and Methods

Cell Culture.

AsPC-1, BxPC-3, Capan-1, MIA PaCa-2 and PANC-1 cells were obtained from ATCC (Manassas, VA, USA) and S2–013 cells have been described previously [29]. Mouse pancreatic cancer cell lines (KPC ((transgenic $KRas^{G12D}$; $Trp^{53R172H}$; Pdx-1 Cre) [30] were generated in the Hollingsworth laboratory. Cells were grown in media (RPMI-1640 for AsPC-1, BxPC-3, MIA PaCa-2, S2–013; DMEM for Capan-1, PANC-1 and KPC) supplemented with heat-inactivated fetal bovine serum (10% for AsPC-1, BxPC-3, Capan-1,

MIA PaCa-2, PANC-1, S2–013; 5% for KPC), glutamine and penicillin-streptomycin at 37°C and 5% CO_2. Mycoplasma testing was performed using MycoAlert mycoplasma detection kit (Lonza, Rockland, ME, USA).

Chemicals.

Brefeldin A and GGTI-2133 were obtained from Sigma-Aldrich (St Louis, MO, USA). Professor David Wiemer at the University of Iowa kindly provided the GGDPSi VSW1198 [8] and RAM2061 [10], as well as the GGTase II inhibitor NHB2005 [31].

Animals.

Female NOD/SCID and C57Bl/6 mice (Charles River) between the ages of 6–8 weeks were housed in the University of Nebraska Medical Center (UNMC) animal facility at a temperature of 23–25 °C, relative humidity of 50–70% and 12/12 hour light/dark cycles. The UNMC IACUC (protocol number 17–119-12-FC) approved all animal studies.

Measurement of intracellular GGPP and FPP.

The quantitation of GGPP and FPP was performed as previously described [32]. In brief, the LC-MS/MS analysis was performed using the Nexera UPLC System connected to a LCMS-8060 (Shimadzu Scientific Instruments, Columbia, MD) with dual ion source. The electrospray ionization source was operated in negative MRM mode. The chromatographic separation and detection of analytes were achieved on a reversed phase ACCQ-TAG Ultra C18 (1.7μm, 100 × 2.1 mm) column (Waters, Inc, Milford, MA). Cells were prepared for analysis by simple protein precipitation using methanol. The mobile phase consisted of A: 10mM ammonium carbonate with 0.1% ammonium hydroxide in water, and B: 0.1% ammonium hydroxide in acetonitrile/methanol (75/25) and the flow rate was set to 0.25 mL/min in gradient condition. The gradient started with 10 % B and increased to 65% B over 7 minutes, then increased to 90 % B at 9.5 minutes then re-equilibrated back to 10% B. The limit of quantification was 0.04 ng/mL for GPP, FPP and GGPP. The assay was linear over the concentration range of 0.04 ng/mL to 20 ng/mL with a total run time of 12 minutes.

MTT assay.

Cells were plated (5000 cells/100 μL per well) in 96-well flat-bottom plates. After 24 hours, drug was added to the wells and the cells were incubated for 72 hours. The MTT assay was performed as previously described [33]. The absorbance obtained from cells treated with solvent only was defined as having an MTT activity of 100%.

Immunoblotting.

PDAC cells were incubated for 48 or 72 hours in the presence or absence of RAM2061. Cells were washed with PBS, and lysed in RIPA buffer supplemented with protease and phosphatase inhibitors (1% sodium deoxycholate, 0.15M NaCl, 0.1% SDS, 1% (v/v) Triton X-100, 0.05 M Tris HCl, pH 7.4). Mouse tissue samples were homogenized with T-PER (Thermo-Scientific, Waltham, MA, USA) supplemented with protease and phosphatase inhibitors. Protein quantification was measured using the BCA method. Equal amounts of total protein were ran on SDS-PAGE gels, transferred to polyvinylidene difluoride

membranes, and probed with primary and secondary antibodies (Supplemental Table 1). An ECL chemiluminescence detection kit and a Bio-Rad ChemiDoc MP imaging system were used to obtain images.

SDS-agarose gel electrophoresis.

Preparation of cell lysates and protein quantification were performed in the same manner as immunoblotting. Equal amounts of protein were loaded onto 1.5% agarose gels and were run in SDS buffer. Proteins were transferred to a PVDF membrane using overnight capillary transfer. An ECL chemiluminescence detection kit and a Bio-Rad ChemiDoc MP imaging system were used to obtain images.

Detection of apoptosis by flow cytometry.

Cells were grown in the presence or absence of RAM2061 for 72 hours. Next, cells were washed with PBS and incubated in 0.25% trypsin for 10 minutes to promote detachment from the plate. Cells were stained with APC-conjugated Annexin V antibody and propidium iodide (PI) according to the manufacturer's recommendations (eBioscience, San Diego, CA, USA). Twenty-thousand cell events were recorded using a BD LSRII flow cytometer. FlowJo software was utilized for all data analysis and generation of flow diagrams. We define early apoptotic cells as being AnnexinV+/PI- and late apoptotic as AnnexinV+/PI+.

Detection of MUC1 by flow cytometry.

MUC1 cell surface levels were measured in BxPC-3 and MIA PaCa-2 cell lines grown in the presence or absence of RAM2061 for 72 hours. Cells were washed with PBS and incubated in 0.25% trypsin for 10 minutes to promote detachment. Next, we washed cells in PBS, re-suspended and incubated for 15 minutes in the presence of MUC1 antibody (clone AR20.5, recognizes the tandem repeat epitope) at a dilution of 1:500 in PBS [34]. AlexaFlour488 anti-mouse (dilution of 1:1000) was used as a secondary antibody. Cells were re-suspended in PBS containing PI. Twenty-thousand cell events were recorded using a BD LSRII flow cytometer. FlowJo software was utilized for all data analysis and generation of flow diagrams. Dead cells (PI+) were gated against so that only live cells were analyzed.

Immunofluorescence microscopy.

Capan-1 cells were plated on coverslips and incubated in the presence or absence of RAM2061 (500 nM) for 72 hours (30,000 cells plated in 2 mL). Cells were fixed in 4% PBS-buffered formalin, blocked and permeabilized in blocking buffers (5% goat serum, 0.2% saponin in PBS), and incubated at room temperature in primary antibody for one hour (dilution of 1:50). Coverslips were washed three times in PBS and incubated in secondary antibody (dilution 1:1000) for 1 hour at room temperature. Coverslips were mounted with VectaShield anti-fade mounting medium with DAPI (Vector Labs, Burlingame, CA, USA). Images were acquired using a Zeiss LSM 710 fluorescent microscope (63X oil immersion lens) and data was analyzed using ZEN 2.1 software.

qRT-PCR.

Cells were incubated for 48 hours in the presence or absence of RAM2061. RNA was isolated using trizol and alcohol precipitation according to manufacturer's instructions (Invitrogen, Carlsbad, CA, USA). RNA (1μg) was reverse transcribed to cDNA using the i-Script cDNA synthesis kit (Bio-Rad, Hercules, CA, USA). cDNA, gene specific primers, and i-Taq Sybr green super mix (Bio-Rad) were mixed according to manufacturer's instruction. qRT-PCR reactions were performed in duplicate in a CFX96 real time machine (Bio-Rad) and data were analyzed using the Bio-Rad CFX manager 3.1 software. Expression values were normalized to the housekeeping gene β-ACTIN. Primer sequences can be found in Supplemental Table 2.

PCR for XBP-1 splicing.

RNA isolation and cDNA synthesis were executed as described above. PCR was performed using XBP-1-specific primers as described by Yan et al [35]. PCR products were separated on a 2% agarose gel, stained with ethidium bromide, and imaged using a UV transilluminator. The upper band denotes unspliced XBP-1 while the lower band denotes spliced XBP-1.

Migration assay.

8.0 μm transwell permeable supports (Corning, Kennebunk, ME, USA) were coated with 125 μg of matrigel (50μL volume, diluted in serum free media). Matrigel was allowed to solidify for 2 hours at 37 degrees. Next, 75,000 AsPC-1 and MIA PaCa-2 cells were plated in serum-free media on the top chamber of the transwell supports. Media with 10% serum was placed in the bottom chamber to serve as a chemoattractant. RAM2061 was added at a final concentration of 250 nM. Following a 48 hour incubation, cells on the top of the membrane were removed and cells on the bottom of the membrane were fixed and stained with Hema3 (Fisher Healthcare, Waltham, MA, USA). Cells were visualized using an inverted light microscope and five randomly chosen fields of view were counted for each transwell.

Ki67 staining.

Tumor tissues were fixed with formalin, imbedded, sectioned, and labeled by Ki67 using standard procedures in the UNMC Tissue Sciences Facility. To estimate proliferation, five random fields of view were chosen from each slide and Ki67 positive cells were counted (n=3 tumors per group).

siRNA knockdown.

Human pancreatic cancer cell lines were treated with DharmaFECT transfection reagent (diluted in serum free media) in presence of either scrambled siRNA or GGDPS siRNA (Dharmacon, Lafayette, CI, USA). Transfection media was removed after 6 hours and replaced with full growth media. After 48 hours, cells were transfected a second time. At 96 hours post the original transfection, cells were lysed and protein was isolated for western blot analysis.

BxPC-3 xenograft model.

BxPC-3 human pancreatic cancer cell lines (5 million cells in 0.1 mL sterile saline mixed 1:1 with matrigel) were subcutaneously inoculated into the flanks of NOD/SCID mice. Treatment with either solvent control (PBS) or VSW1198 (0.1mg/kg twice weekly via tail vein) began once the mice established palpable tumors (~100 mm^3). Mice were divided into control and treatment groups to provide an equal distribution of tumor size for each group at the start of treatment (n=5 each). Efficacy was determined by measuring primary tumor volume three times a week using a caliper. The following equation was used to calculate tumor volume: $4\pi/3 \times (\text{width}/2)2 \times (\text{length}/2)$.

KPC orthotopic model.

KPC mouse pancreas tumor cell lines derived in-house were used for the orthotopic tumor transplantation studies. Cells (7,500 cells in 30 μL sterile saline) were injected orthotopically into the pancreata of wild type C57Bl/6 mice (n=20). Three mice were lost during orthotopic injections due to complications from anesthesia. Mice were divided into two groups (n=9 for treatment and n=8 for control). When tumors reached ~5 mm^3 (~10 days after transplantation and determined by ultrasound), mice were injected in the intraperitoneal cavity with either solvent control (PBS) or 0.1 mg/kg VSW1198 two times a week until mice became moribund. Tumor weight was recorded at time of sacrifice.

Statistics.

Two-tailed t-tests were used to calculate statistical significance between control and treated groups. Linear mixed models were used to compare tumor volumes from the BxPC-3 xenograft model over time. The model included fixed effects for group, day and the group x day interaction, where day is modeled as categorical. A first-order autoregressive covariance structure was used to model the covariance structure. The Bonferroni method corrected for multiple comparisons between groups at each time point and to adjust multiple dose comparisons to control. An α of 0.05 was set as the level of significance. SAS software version 9.4 was used for fitting the linear mixed model (SAS Institute Inc., Cary, NC). Variance was similar between the groups being statistically compared.

Post-hoc power calculation for the BxPC-3 xenograft model showed 80% power with n=5 mice per group to detect a 100mm^3 difference in tumor volume with group standard deviations of 33.5mm^3, using a two-sided t-test at 8 time points, and α=0.05/8=0.006 to adjust for 8 pairwise comparisons at the different time points. A power calculation for the KPC orthotopic mouse study showed 87% power with n=8 mice per group to detect a 0.5g difference in tumor weight with group standard deviations of 0.3g, with α=0.05 using a two-sided t-test.

Supplementary Material

Refer to Web version on PubMed Central for supplementary material.

Acknowledgements.

This work was supported by the Fred & Pamela Buffett Cancer Center Support Grant from the National Cancer Institute under award P30 CA036727 and the National Institutes of Health P50CA127297. The authors wish to acknowledge the support of the Fred & Pamela Buffett Cancer Center Advanced Microscopy Core Facility and the Flow Cytometry Research Facility, supported by the National Cancer Institute under award P30 CA036727. We thank Janice A. Taylor and James R. Talaska of the Advanced Microscopy Core Facility for providing assistance with confocal microscopy.

References.

1. Luberice K, Downs D, Sadowitz B, Ross S, Rosemurgy A. Has survival improved following resection for pancreatic adenocarcinoma? Am J Surg 2017; 214: 341–6. [PubMed: 28601189]
2. Suh H, Pillai K, Morris DL. Mucins in pancreatic cancer: biological role, implications in carcinogenesis and applications in diagnosis and therapy. Am J Cancer Res 2017; 7: 1372–83. [PubMed: 28670497]
3. Besmer DM, Curry JM, Roy LD, Tinder TL, Sahraei M, Schettini J, et al. Pancreatic ductal adenocarcinoma mice lacking mucin 1 have a profound defect in tumor growth and metastasis. Cancer Res 2011; 71: 4432–42. [PubMed: 21558393]
4. Jonckheere N, Skrypek N, Van Seuningen I. Mucins and tumor resistance to chemotherapeutic drugs. Biochim Biophys Acta 2014; 1846: 142–51. [PubMed: 24785432]
5. Kaur S, Kumar S, Momi N, Sasson AR, Batra SK. Mucins in pancreatic cancer and its microenvironment. Nature reviews Gastroenterology & hepatology 2013; 10: 607–20. [PubMed: 23856888]
6. Taylor-Papadimitriou J, Burchell JM, Graham R, Beatson R. Latest developments in MUC1 immunotherapy. Biochem Soc Trans 2018; 46: 659–68. [PubMed: 29784646]
7. Haney SL, Wills VS, Wiemer DF, Holstein SA. Recent advances in the development of mammalian geranylgeranyl diphosphate synthase inhibitors. Molecules 2017; 22: 886.
8. Wills VS, Allen C, Holstein SA, Wiemer DF. Potent triazole bisphosphonate inhibitor of geranylgeranyl diphosphate synthase. ACS Med Chem Lett 2015; 6: 1195–8. [PubMed: 26713103]
9. Haney SL, Chhonker YS, Varney ML, Talmon G, Murry DJ, Holstein SA. Preclinical investigation of a potent geranylgeranyl diphosphate synthase inhibitor. Invest New Drugs 2018.
10. Matthiesen RA, Varney ML, Xu PC, Rier AS, Wiemer DF, Holstein SA. alpha-Methylation enhances the potency of isoprenoid triazole bisphosphonates as geranylgeranyl diphosphate synthase inhibitors. Bioorg Med Chem 2018; 26: 376–85. [PubMed: 29248353]
11. Holstein SA, Hohl RJ. Isoprenoid biosynthetic pathway inhibition disrupts monoclonal protein secretion and induces the unfolded protein response pathway in multiple myeloma cells. Leuk Res 2011; 35: 551–9. [PubMed: 20828814]
12. Born EJ, Hartman SV, Holstein SA. Targeting HSP90 and monoclonal protein trafficking modulates the unfolded protein response, chaperone regulation and apoptosis in myeloma cells. Blood Cancer J 2013; 3: e167. [PubMed: 24317089]
13. Sorensen AL, Reis CA, Tarp MA, Mandel U, Ramachandran K, Sankaranarayanan V, et al. Chemoenzymatically synthesized multimeric Tn/STn MUC1 glycopeptides elicit cancer-specific anti-MUC1 antibody responses and override tolerance. Glycobiology 2006; 16: 96–107. [PubMed: 16207894]
14. Taylor-Papadimitriou J, Peterson JA, Arklie J, Burchell J, Ceriani RL, Bodmer WF. Monoclonal antibodies to epithelium-specific components of the human milk fat globule membrane: production and reaction with cells in culture. Int J Cancer 1981; 28: 17–21. [PubMed: 7309278]
15. Hanson RL, Hollingsworth MA. Functional Consequences of Differential O-glycosylation of MUC1, MUC4, and MUC16 (Downstream Effects on Signaling). Biomolecules 2016; 6.
16. Misumi Y, Miki K, Takatsuki A, Tamura G, Ikehara Y. Novel blockade by brefeldin A of intracellular transport of secretory proteins in cultured rat hepatocytes. J Biol Chem 1986; 261: 11398–403. [PubMed: 2426273]
17. Deer EL, Gonzalez-Hernandez J, Coursen JD, Shea JE, Ngatia J, Scaife CL, et al. Phenotype and genotype of pancreatic cancer cell lines. Pancreas 2010; 39: 425–35. [PubMed: 20418756]

18. Yu DC, Liu J, Chen J, Shao JJ, Shen X, Xia HG, et al. GGPPS1 predicts the biological character of hepatocellular carcinoma in patients with cirrhosis. BMC Cancer 2014; 14: 248. [PubMed: 24716791]
19. Igarashi T, Araki K, Yokobori T, Altan B, Yamanaka T, Ishii N, et al. Association of RAB5 overexpression in pancreatic cancer with cancer progression and poor prognosis via E-cadherin suppression. Oncotarget 2017; 8: 12290–300. [PubMed: 28103577]
20. Li Y, Sun X, Ji D, Kong X, Liu D, Zhao Z, et al. Expression of Rab5a correlates with tumor progression in pancreatic carcinoma. Virchows Arch 2017; 470: 527–36. [PubMed: 28243729]
21. Nath S, Mukherjee P. MUC1: a multifaceted oncoprotein with a key role in cancer progression. Trends Mol Med 2014; 20: 332–42. [PubMed: 24667139]
22. Liu X, Yuan Z, Chung M. MUC1 intra-cellular trafficking is clathrin, dynamin, and rab5 dependent. Biochem Biophys Res Commun 2008; 376: 688–93. [PubMed: 18812166]
23. Jin C, Rajabi H, Pitroda S, Li A, Kharbanda A, Weichselbaum R, et al. Cooperative interaction between the MUC1-C oncoprotein and the Rab31 GTPase in estrogen receptor-positive breast cancer cells. PLoS One 2012; 7: e39432. [PubMed: 22792175]
24. Kinlough CL, McMahan RJ, Poland PA, Bruns JB, Harkleroad KL, Stremple RJ, et al. Recycling of MUC1 is dependent on its palmitoylation. J Biol Chem 2006; 281: 12112–22. [PubMed: 16507569]
25. Kaur S, Kumar S, Momi N, Sasson AR, Batra SK. Mucins in pancreatic cancer and its microenvironment. Nat Rev Gastroenterol Hepatol 2013; 10: 607–20. [PubMed: 23856888]
26. Wissniowski TT, Meister S, Hahn EG, Kalden JR, Voll R, Ocker M. Mucin production determines sensitivity to bortezomib and gemcitabine in pancreatic cancer cells. Int J Oncol 2012; 40: 1581–9. [PubMed: 22266985]
27. Marten A, Zeiss N, Serba S, Mehrle S, von Lilienfeld-Toal M, Schmidt J. Bortezomib is ineffective in an orthotopic mouse model of pancreatic adenocarcinoma. Mol Cancer Ther 2008; 7: 3624–31. [PubMed: 19001444]
28. Wang H, Cao Q, Dudek AZ. Phase II study of panobinostat and bortezomib in patients with pancreatic cancer progressing on gemcitabine-based therapy. Anticancer Res 2012; 32: 1027–31. [PubMed: 22399627]
29. Iwamura T, Taniguchi S, Kitamura N, Yamanari H, Kojima A, Hidaka K, et al. Correlation between CA19–9 production in vitro and histological grades of differentiation in vivo in clones isolated from a human pancreatic cancer cell line (SUIT-2). J Gastroenterol Hepatol 1992; 7: 512–9. [PubMed: 1391733]
30. Hingorani SR, Wang L, Multani AS, Combs C, Deramaudt TB, Hruban RH, et al. Trp53R172H and KrasG12D cooperate to promote chromosomal instability and widely metastatic pancreatic ductal adenocarcinoma in mice. Cancer Cell 2005; 7: 469–83. [PubMed: 15894267]
31. Coxon FP, Joachimiak L, Najumudeen AK, Breen G, Gmach J, Oetken-Lindholm C, et al. Synthesis and characterization of novel phosphonocarboxylate inhibitors of RGGT. Eur J Med Chem 2014; 84: 77–89. [PubMed: 25016230]
32. Chhonker YS, Haney SL, Bala V, Holstein SA, Murry DJ. Simultaneous Quantitation of Isoprenoid Pyrophosphates in Plasma and Cancer Cells Using LC-MS/MS. Molecules 2018; 23.
33. Holstein SA, Hohl RJ. Interaction of cytosine arabinoside and lovastatin in human leukemia cells. Leuk Res 2001; 25: 651–60. [PubMed: 11397469]
34. Qi W, Schultes BC, Liu D, Kuzma M, Decker W, Madiyalakan R. Characterization of an anti-MUC1 monoclonal antibody with potential as a cancer vaccine. Hybrid Hybridomics 2001; 20: 313–24. [PubMed: 11839249]
35. Yan Y, Gao YY, Liu BQ, Niu XF, Zhuang Y, Wang HQ. Resveratrol-induced cytotoxicity in human Burkitt's lymphoma cells is coupled to the unfolded protein response. BMC Cancer 2010; 10: 445. [PubMed: 20723265]

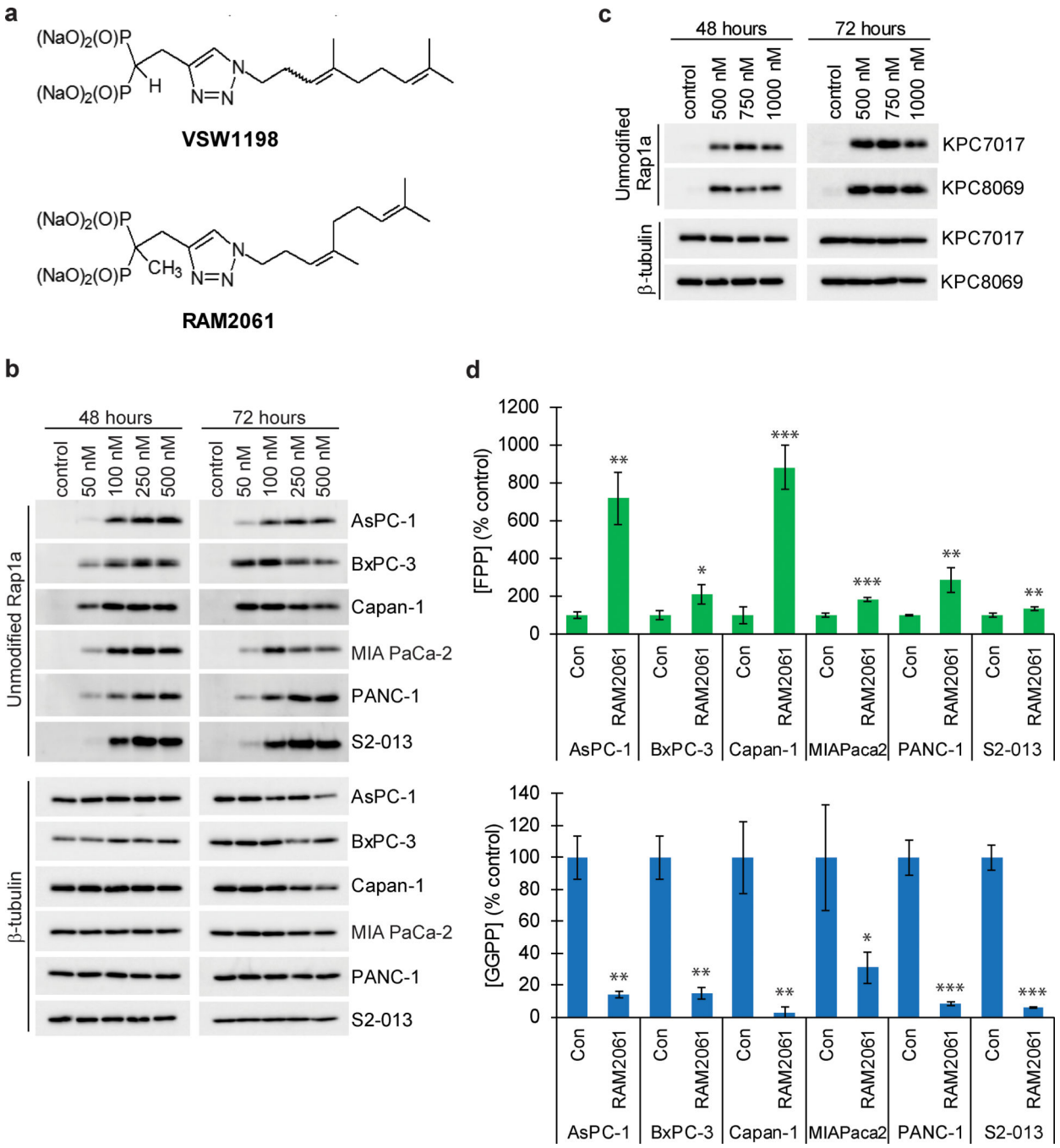

Fig. 1. RAM2061 inhibits GGDPS in human and mouse PDAC cell lines.

a Chemical structure of the two GGDPS inhibitors used in these studies, VSW1198 and RAM2061. **b** and **c** Immunoblot analysis showing unmodified Rap1a in human (b) and mouse (c) PDAC cell lines treated with increasing concentrations of RAM2061 for 48 or 72 hours. β-tubulin is shown as a loading control. Immunoblots are representative of three independent experiments. **d** Levels of FPP and GGPP in human PDAC cell lines grown in the presence or absence of RAM2061 for 48 hours. ($n = 3$, data are displayed as mean ± stdev, *denotes $p < 0.05$. **denotes $p < 0.01$. ***denotes $p < 0.001$).

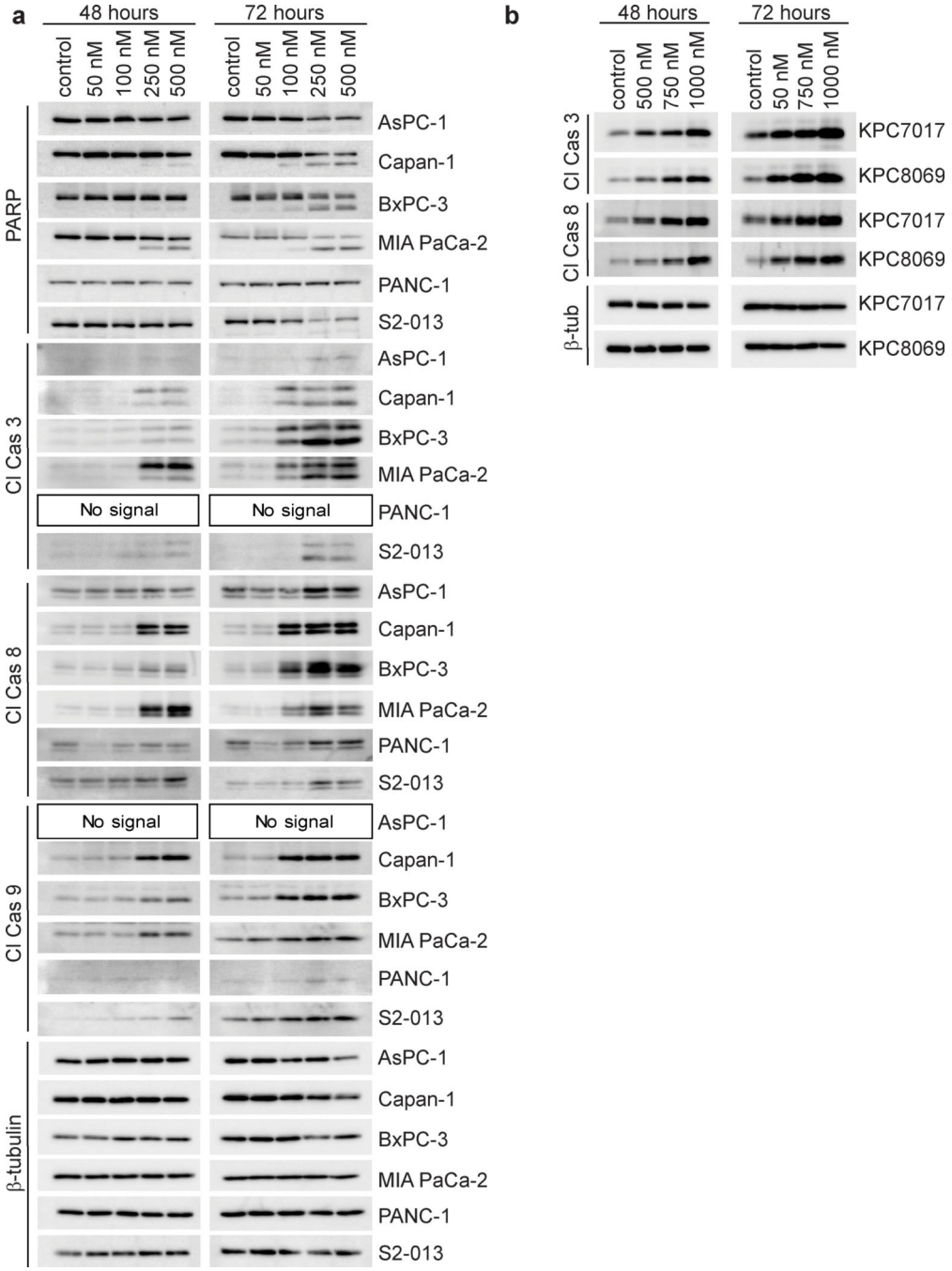

Fig. 2. Inhibition of GGDPS induces markers of apoptosis in PDAC cell lines.

a and **b** Immunoblot analysis showing protein levels of apoptotic markers in human (a) and mouse (b) PDAC cell lines treated with or without RAM2061 for 48 or 72 hours. β-tubulin is shown as a loading control. Immunoblots are representative of three independent experiments.

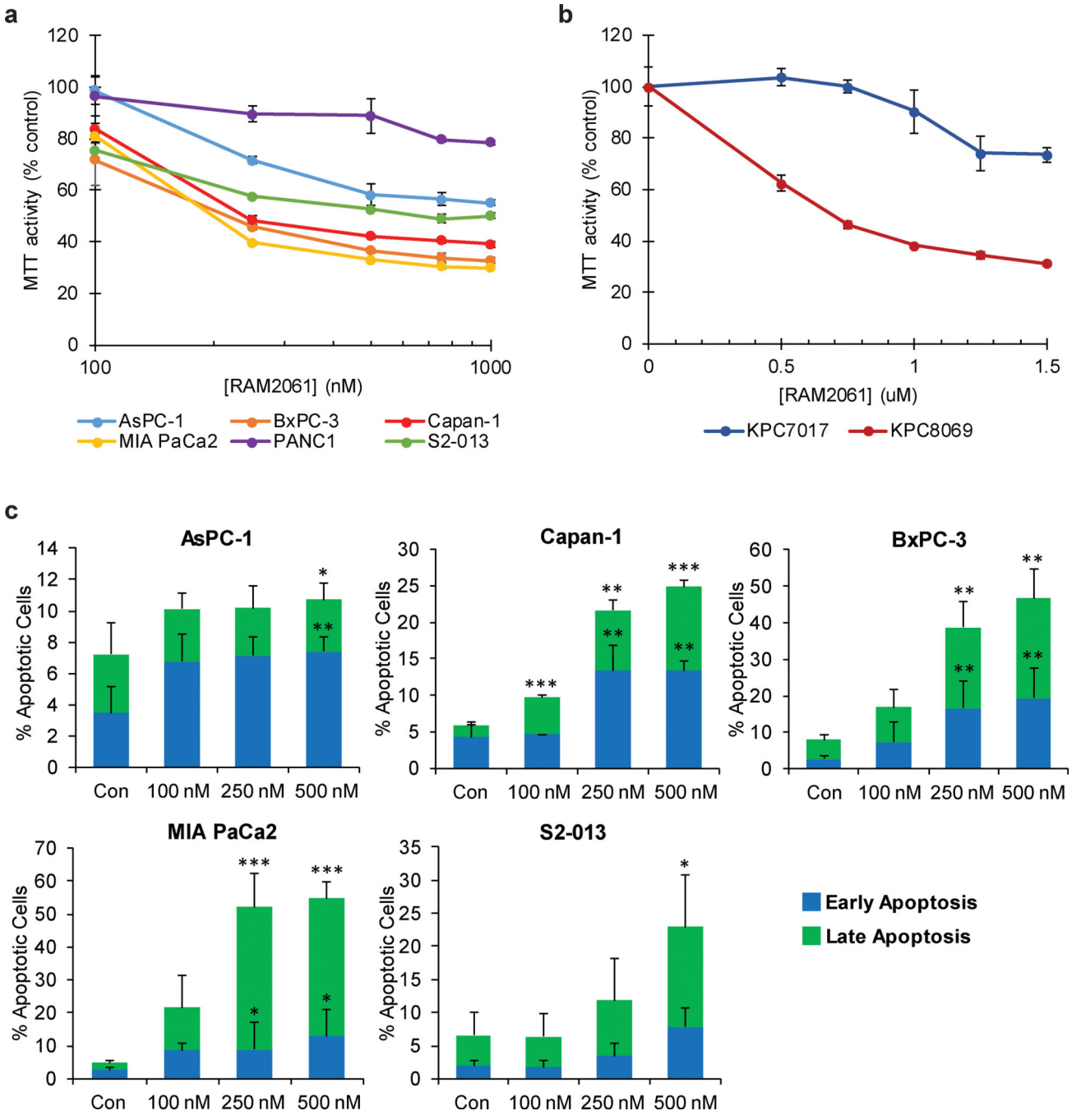

Fig. 3. Treatment of PDAC cells with GGDPSi triggers apoptotic cell death.

a and **b** MTT assays were performed following a 72-hour incubation period with RAM2061 in six human (a) and two mouse (b) PDAC cell lines (n=4, data are displayed as mean ± stdev). **c** Human PDAC cells were treated with or without RAM2061 for 72 hours. Cells were stained with fluorescently conjugated Annexin V and propidium iodide (PI) and analyzed by flow cytometry. Data are expressed as the average percentage of Annexin V +/PI- (early apoptotic) and AnnexinV+PI+ (late apoptotic) ($n = 3$, data are displayed as mean ± stdev, *denotes $p < 0.05$. **denotes $p < 0.01$. ***denotes $p < 0.001$).

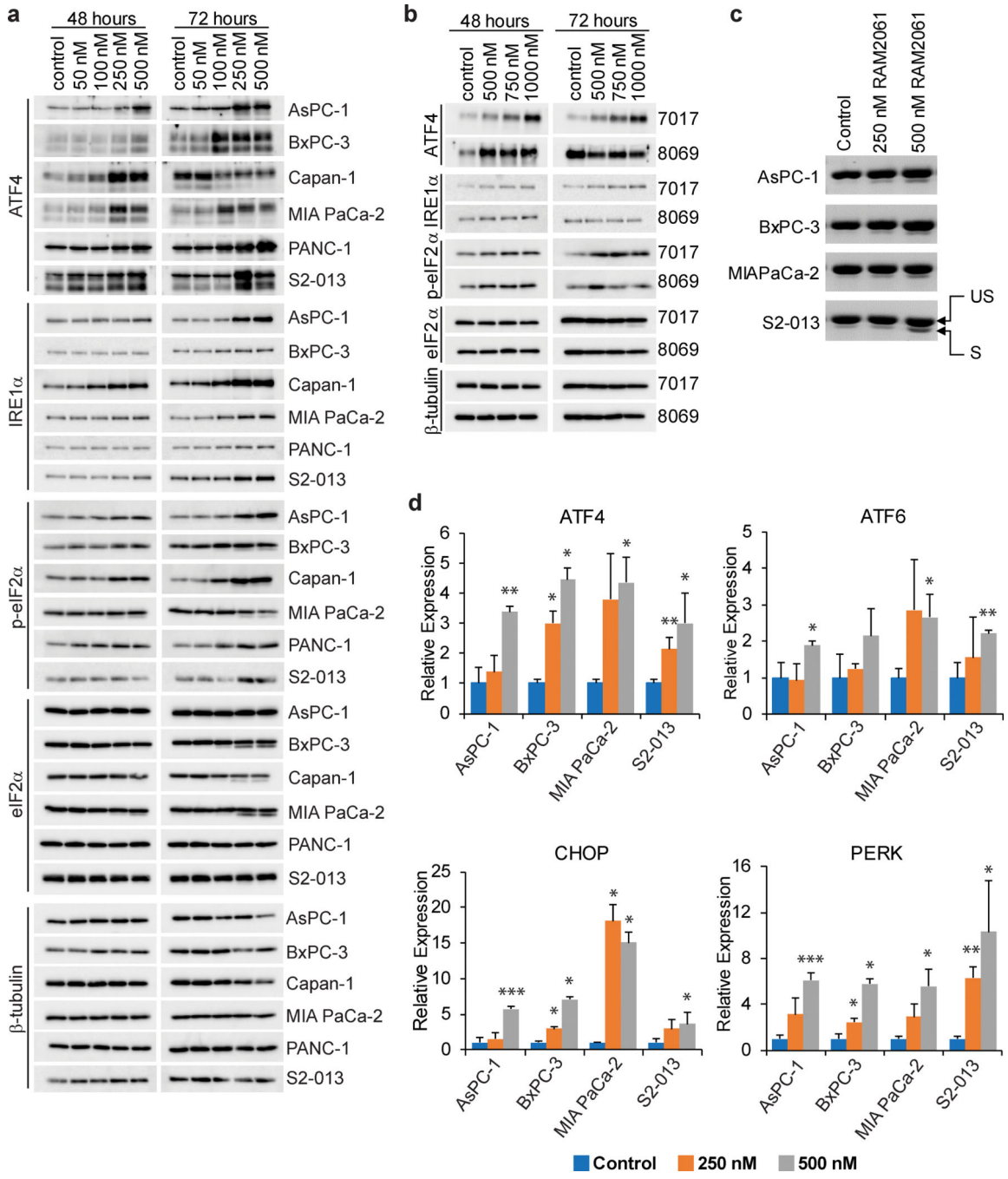

Fig. 4. GGDPS inhibition activates the UPR pathway.

a and **b** Immunoblot analysis showing protein levels of UPR markers in six human (a) and two mouse (b) PDAC cell lines treated with or without RAM2061 for 48 or 72 hours. Mouse KPC8069 cells are denoted as 8069 and KPC7017 are denoted 7017. β-tubulin is shown as a loading control. Immunoblots are representative of three independent experiments. **c** Human PDAC cells were incubated for 48 hours with or without RAM2061. PCR was performed using XBP-1-specific primers. The upper band represents unspliced XBP-1 (US) and the lower band represents spliced XBP-1 (S). **d** qRT-PCR analysis of ATF4, ATF6, CHOP and

PERK expression in human PDAC cells incubated in the presence or absence of RAM2061 (48 hour incubation). Data represents fold change normalized to control ($n = 3$, data are displayed as mean ± SEM, *denotes $p < 0.05$. **denotes $p < 0.01$. ***denotes $p < 0.001$).

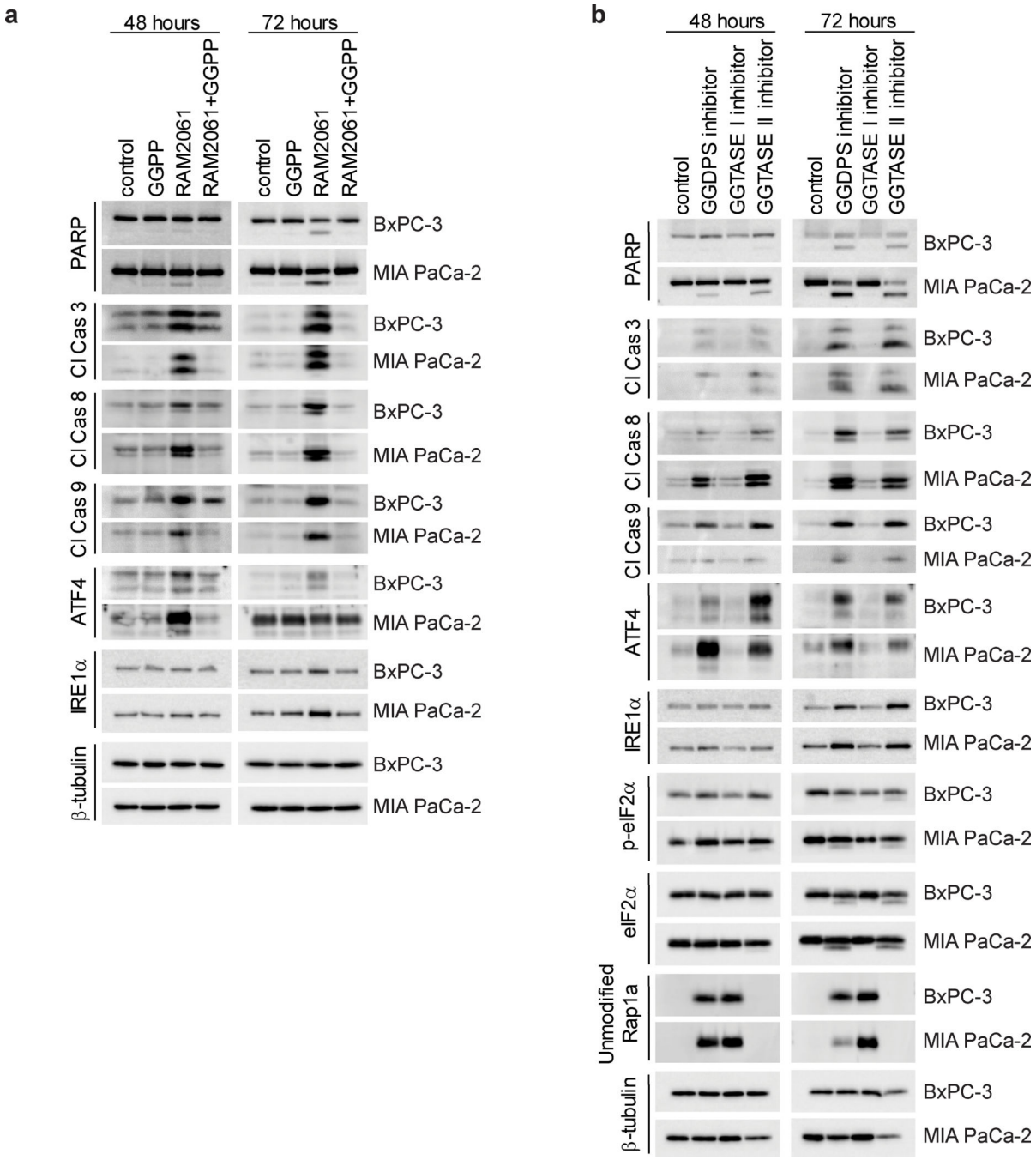

Fig. 5. Reduction in cellular GGPP and inhibition of Rab activity mediate RAM2061-induced UPR and apoptosis activation.

Immunoblot analysis showing protein levels of apoptotic and UPR markers as well as unmodified Rap1a in MIA PaCa-2 and BxPC-3 cell lines. β-tubulin is shown as a loading control. Immunoblots are representative of three independent experiments. **a** PDAC cells were grown in the presence or absence of RAM2061 (250 nM) with or without the addition of 10 μM GGPP. **b** PDAC cells were grown in the presence or absence of a GGDPS inhibitor (RAM2061, 250 nM) GGTase I inhibitor (GGTI-2133, 25 μM) or a GGTase II inhibitor (NHB2005, 2.5 mM) for 48 or 72 hours.

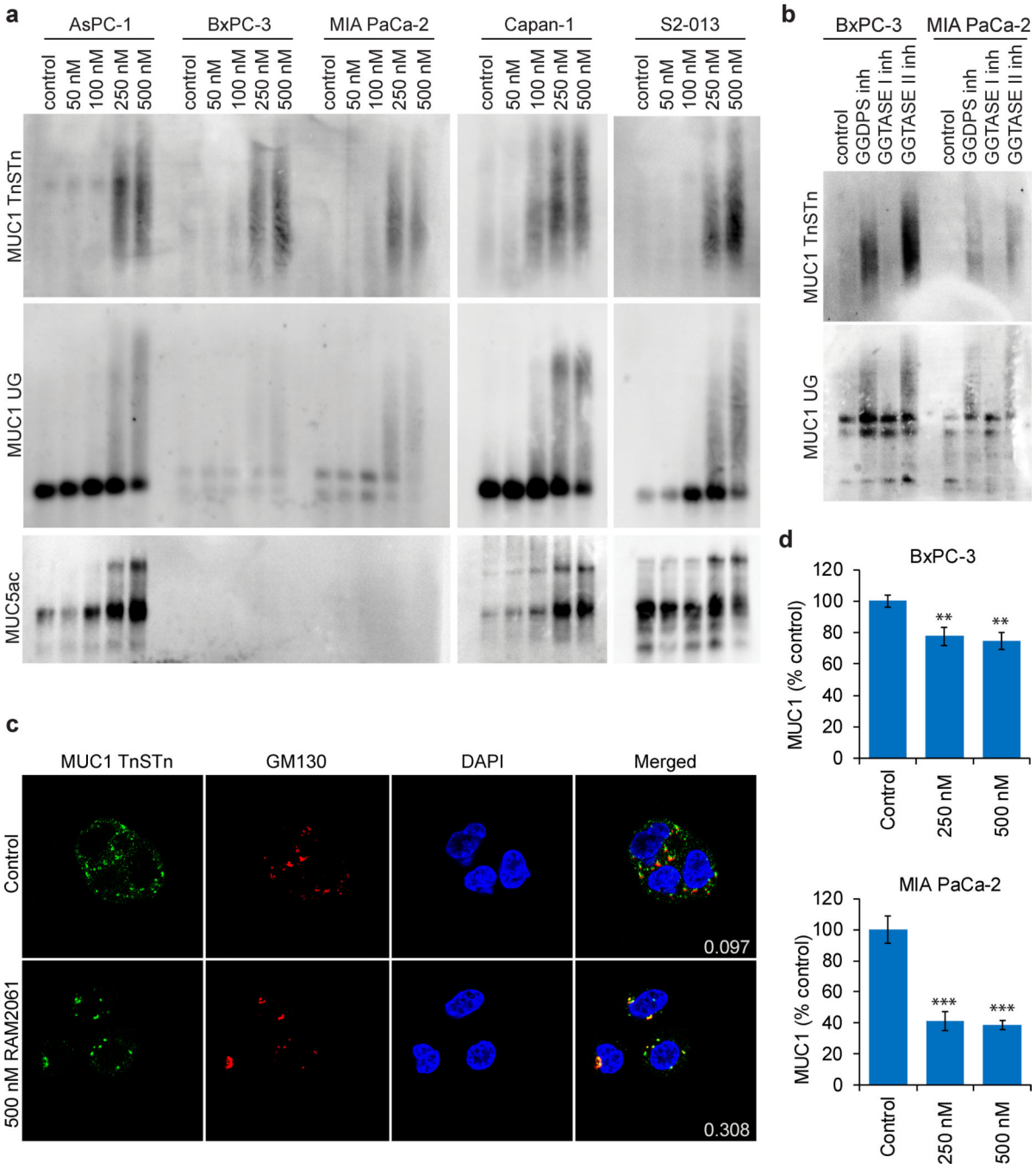

Fig. 6. Inhibition of Rab geranylgeranylation disrupts mucin trafficking.

a Immunoblot analysis showing protein levels of MUC1 and MUC5ac in human PDAC cell lines incubated in the presence or absence of RAM2061 for 48 hours. Immunoblots were performed to detect two different epitopes of MUC1 (TnSTn and under-glycosylated (UG)). Immunoblots are representative of three independent experiments. **b** BxPC-3 and MIA PaCa-2 cells were incubated for 48 hours in the presence of a GGDPS inhibitor (RAM2061, 250 nM) GGTase I inhibitor (GGTI-2133, 25 μM) or a GGTase II inhibitor (NHB2005, 2.5 mM). **c** Fluorescence microscopy images of Capan-1 cells treated with or without 500 nM

RAM2061 for 72 hours. Cells were fixed and stained with antibodies against MUC1 (TnSTn antigen), GM130 (Golgi label), and DAPI (nucleus label). Overlap of red and green channels is shown in the merged images. The Mander's overlap coefficient shows the relative proportion of MUC1 that co-localize with the Golgi (# green colocalized pixels/total # green pixels). Representative images are shown. **d** Flow cytometry analysis of MUC1 cell surface levels in BxPC-3 and MIA PaCa-2 cell lines. Cells were incubated in the presence or absence of RAM2061 for 72 hours. Data are normalized to control. ($n = 3$, data are displayed as mean ± stdev, **denotes $p < 0.01$. ***denotes $p < 0.001$).

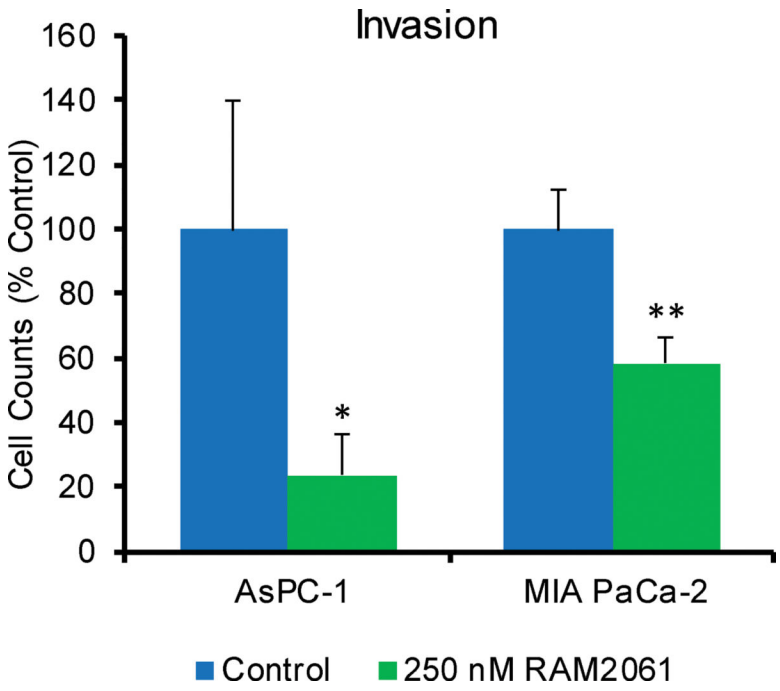

Fig. 7. GGDPS inhibition inhibits cell invasion.

AsPC-1 and MIA PaCa-2 cells were seeded on matrigel-coated transwells and grown in the presence or absence of RAM2061. After 48 hours, cells on the bottom of the transwells were counted. Data are normalized to control. ($n = 3$, data are displayed as mean ± stdev, *denotes $p < 0.05$. **denotes $p < 0.01$).

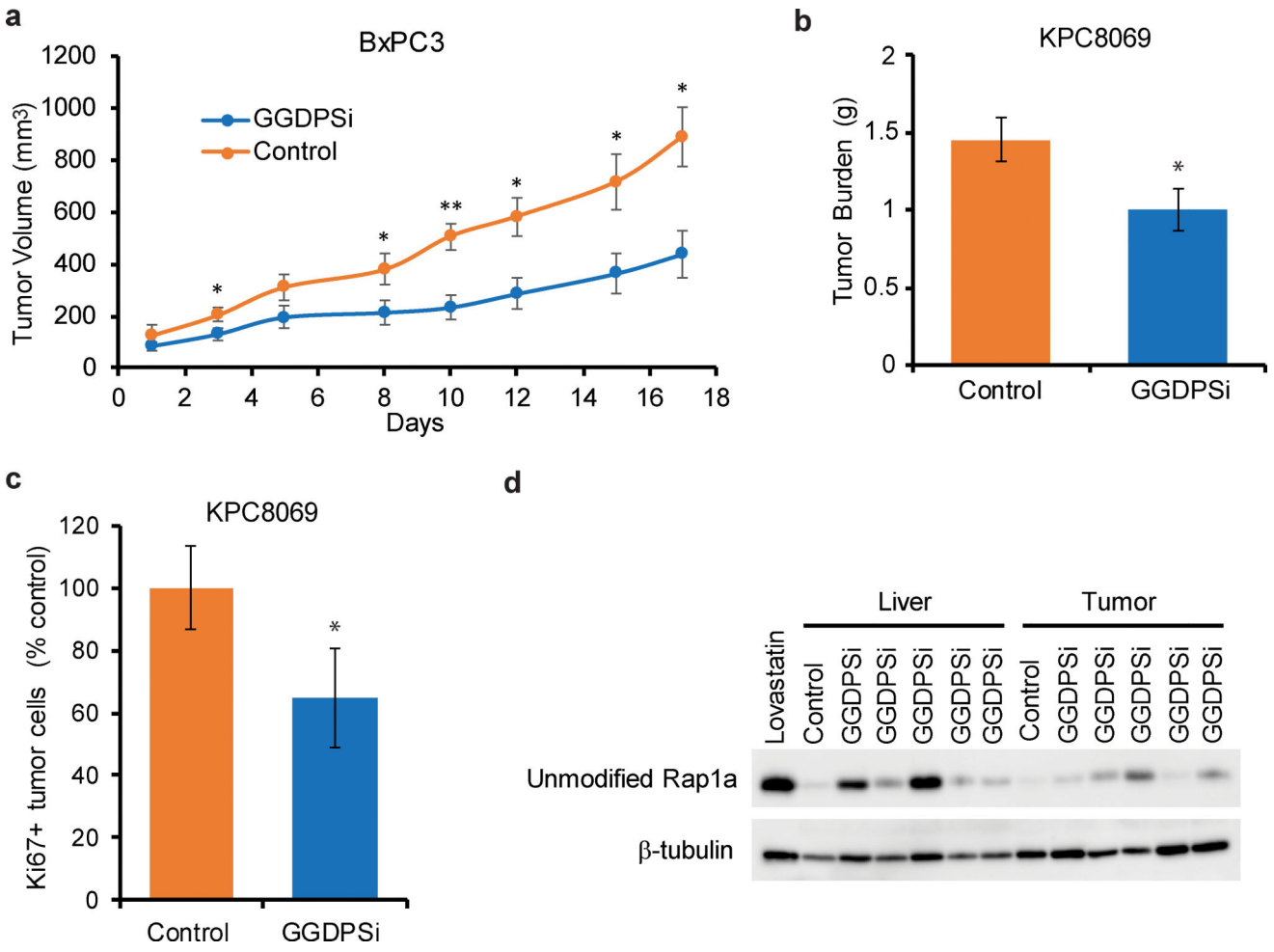

Fig. 8. GGDPSi treatment slows PDAC tumor growth *in vivo*.

a Tumor growth curves for BxPC-3 flank xenografts. Mice were treated twice weekly with either solvent only control (PBS) or a GGDPSi (VSW1198). (n = 5 mice per group, data are displayed as mean ± SEM, *denotes $p < 0.05$. **denotes $p < 0.01$). **b** Tumor burden for the KPC orthotopic mouse model at the time of sacrifice. Mice were treated twice weekly with either solvent only control (PBS) or GGDPSi (VSW1198). (n = 8 for control and n=9 for treatment groups, data are displayed as mean ± SEM, *denotes $p < 0.05$). **c** Cellular proliferation in tumors as measured by ki67 staining for the KPC orthotopic mouse model at the time of sacrifice. Data are shown as mean normalized to control. (n=3 per group, error bars denote standard deviation, *denotes $p < 0.05$). **d** Immunoblot analysis showing unmodified Rap1a in tumor and liver lysates prepared from the KPC orthotopic mouse model. Mice were treated with either PBS (control) or VSW1198 (GGDPSi). The positive control was generated from a cell line treated with lovastatin. β-tubulin is shown as a loading control.